On the selective deposition of tin and tin oxide on various glasses using a high power diode laser

J. Lawrence*, P. Lubrani, L. Li

Laser Processing Research Centre, Department of Mechanical Engineering, University of Manchester Institute of Science and Technology (UMIST), Manchester M60 1QD, UK

Abstract

The deposition of SnO_2 using a 120-W high power diode laser (HPDL) on both fused silica and soda-lime−silica glass has been successfully demonstrated. Deposition on both glass substrates was carried out with laser power densities of 650−1600 W cm^{-2} and at rates of 420−1550 mm min^{-1}. The thickness of the deposited layers was typically approximately 250 μm. The maximum theoretical coverage rate that it may be possible to achieve using the HPDL was calculated as being 3.72 m^2 h^{-1}. Owing to the wettability characteristics of Sn, it proved impossible to deposit the metal on either glass substrate. Evidence of solidified microstructures was observed, with the microstructures differing considerably across the same deposited track. These differences were attributed to variations in the solidification rate, R, and the thermal gradient, G. Adhesion of the SnO_2 with the soda-lime−silica glass was found to be due to mechanical bonding. The adhesion of the SnO_2 with the fused silica was seen to be the result of a chemical bond arising from an interface region between the SnO_2 and the fused silica glass substrate. This interface region was found to be comprised of mainly Si and rich with Sn_3O_4. © 2001 Elsevier Science B.V. All rights reserved.

1. Introduction

Glass is mainly used as a substrate material due to its advantages over polymers and metals, namely its high strength and generally lighter weight as compared to metallic materials. It also retains its strength to relatively higher temperatures and is less susceptible to oxidation and corrosion at these elevated temperatures. However, it is primarily the optical properties of glass which make the material interesting to use and therefore coat. Another main advantage of glass, in terms of material deposition, is its ability to cope with the stresses created by the adhering of a new atomic structure.

Thin films of optical and ferro-electric materials have acquired considerable importance in recent times in view of their impact on the emerging as well as future technologies. Films of SnO_2, for example, have gained importance because of their use in opto-electronic devices, solar energy converters, light-transmitting electrodes, liquid crystals, heat mirrors, gas sensors, etc. [1]. SnO_2 has traditionally been coated onto glass mainly as a base for glass-to-metal seals due to its good wetting behaviour [2]. Within the electronics industry the deposition of SnO_2 on glass has found many uses, primarily nowadays being used on inorganic glasses to produce LCD displays on portable computers [3]. Thin SnO_2 films are also used extensively in solar energy converters as conducting buffer layers to improve electric conductivity with low resistivity [4]. Within the aerospace industry, SnO_2 is coated onto various plastic substrates. This coating can range from high resistance

* Corresponding author. Tel.: +44-161-200-3806, ext. 3806; fax: +44-161-200-3803.

E-mail address: j.lawrence@umist.ac.uk (J. Lawrence).

coatings on polyamide film or FEP film, for static dissipative uses as resistant static discharges. The coatings are also used for electromagnetic interference shielding on windows [5]. A limited amount of evidence of the application of Sn and SnO_2 coatings in fields of gas sensing [6], biomedicine [7] and the automotive industry [8] can also be found.

At present, the coating of Sn and SnO_2 on glass for the above applications has traditionally been achieved by means of a number of mechanisms: sputtering, spin deposition and plasma spraying [9,10], and physical methods: ion implantation and sol–gel processing [11,12]. In more recent times, however, the use of lasers to directly and indirectly melt and fuse metals onto many substrates, including glass, has been investigated. The laser deposition of Sn and SnO_2 on glass derives from the need to control the interface between the two surfaces. Consequently the laser is an ideal tool for this task since it can deliver a high power beam to the interface without changing the bulk substrate dramatically [13]. Both laser chemical vapour deposition (LCVD) [14] and laser physical vapour deposition (LPVD) [15] have been shown to be viable techniques. Pulsed laser deposition (PLD) has been employed successfully to deposit thin films (100–1000 Å) of indium tin oxide (ITO) onto glass substrates with a KrF excimer laser [16]. The laser spraying of metallic particles onto various substrates has been studied [17], but the technique is not without attendant problems as the particles require certain properties for the phenomenon of evaporation induced propulsion to be realised. The possibility of pre-placed powder deposition with CO_2 and Nd:YAG lasers has also been investigated [17]. However, due to the lasers' characteristics, much difficulty in achieving low dilution fusion because of the small operating window was experienced.

This present work describes the hitherto unreported successful demonstration of the selective deposition of a relatively thick tin oxide layer on ubiquitous soda-lime–silica glass and fused silica glass using a HPDL in normal atmospheric conditions. The required laser operating parameters are given. Furthermore, the bonding and adhesion mechanisms involved in the process are comprehensively investigated, thus elucidating the reasons for successful deposition. It is believed that the technique presented in this paper is a useful addition to the burgeoning applications base of the HPDL.

2. Experimental procedures

The laser used in the study was a surgical HPDL (Diomed, Inc.), emitting at 940 nm and operating in the continuous wave (CW) mode with rated optical powers ranging from 0 to 120 W. The HPDL beam was deliv-
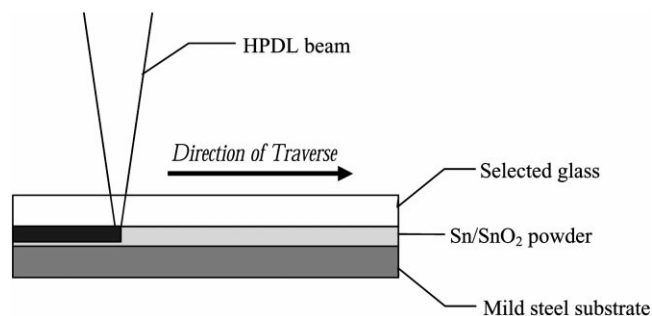

Fig. 1. Experimental arrangement for the deposition of Sn and SnO_2 on the selected glasses.

ered to the work area by means of a 4-m-long, 600-μm core diameter optical fibre, the end of which was connected to a 2:1 focusing lens assembly mounted on the z-axis of a three-axis CNC gantry table. The samples were irradiated using the defocused high order mode HPDL beam with a beam spot diameter of 2 mm and laser powers (measured at the workpiece using a Power Wizard power meter) of 10–55 W. The defocused HPDL beam was fired across the surfaces of the glasses selected with the Sn and SnO_2 pre-placed beneath on a mild steel substrate as shown in Fig. 1. The HPDL beam was traversed over the surfaces of the samples using the x- and y-axis of the CNC gantry table at speeds ranging from 240 to 1440 mm min^{-1}. The laser optics were protected by means of a coaxially blown O_2 shield gas jet at a rate of 3 l min^{-1}. The glasses used as substrates for the work were fused silica glass (99.9% fused) and the common soda-lime–silica glass. The metals deposited on the glasses were pure Sn and SnO_2 (Sn 78.77 wt.%, O_2 21.23 wt.%).

3. Deposition of SnO_2 on fused silica and soda-lime–silica glass

3.1. Operating window

Fig. 2 depicts a schematic representation of the operating window for the deposition of SnO_2 on both fused silica and soda-lime–silica glass. Within the optimum operating conditions (shaded area), the deposition of lines of SnO_2 which adhered well to the glass were possible. Furthermore, from Fig. 2 it is possible to ascertain the maximum deposition/coverage rate that it may be possible to achieve using the HPDL. This was calculated as being 3.72 m^2 h^{-1} for a circular beam of 4 mm diameter with a laser power of 110 W and a traverse speed of 1550 mm min^{-1}.

3.2. Morphological characteristics
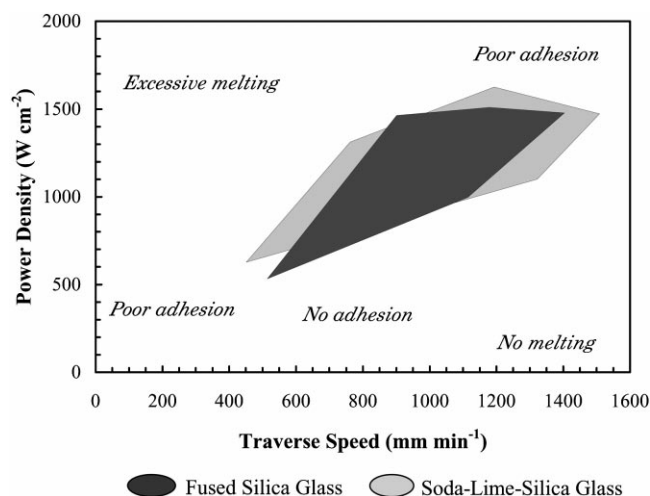
The typical surface morphology of deposited tracks

Fig. 2. Schematic representation of the operating window for the deposition of SnO$_2$ on fused silica and soda-lime−silica glass using the 120-W HPDL.

Fig. 4. Typical SEM cross-sectional images of SnO$_2$ deposited on (a) fused silica and (b) soda-lime−silica glass.

soda-lime−silica glass is shown in Fig. 4. Both Fig. 4a,b shows clearly that the deposited SnO$_2$ layer seems to be well bonded to the glass substrates. However, the methods of bonding between the SnO$_2$ and the two substrates appear to be very different. From Fig. 4a it is possible to clearly discern an interface region between the SnO$_2$ and the fused silica glass substrate, while in Fig. 4b the SnO$_2$ layer appears to be mechanically bonded to the soda-lime−silica substrate.

of SnO$_2$ on (a) fused silica and (b) soda-lime−silica glass is shown in Fig. 3. As is evident from Fig. 3a, the surface of the deposited SnO$_2$ tracks on the fused silica glass appear to be slightly undulated, with the undulations being regular in both periodicity and intensity. In addition, the surface displays very few microcracks and no porosities. In contrast, Fig. 3b shows that the surface of the deposited SnO$_2$ tracks on the soda-lime−silica glass are considerably more irregular and uneven. In Fig. 3a the solidification structure appears to be of a directional nature. This directional solidification structure was seen typically to extend in a perpendicular direction from the edges of the laser melt track, tending inwards towards the centre of the track. As one can see from Fig. 3b, cracking of the surface of the deposited SnO$_2$ tracks was an attendant problem. Cracks were found to occur in both the deposited SnO$_2$ tracks and the soda-lime−silica glass substrate.

4. Deposition of Sn on fused silica and soda-lime−silica glass

Regardless of the HPDL operating parameters, it proved impossible to deposit pure Sn on either a fused silica glass substrate or a common soda-lime−silica glass substrate. Indeed, HPDL interaction with the Sn when placed on the surface of the soda-lime−silica glass simply resulted in the 'balling' of the Sn; the formation of small spheres approximately the diameter of the laser beam itself. Indeed, such observations are in accord with those of Bourell et al. [18] and Agarwala et al. [19], who noted the balling phenomena during the laser sintering of ceramic powders. Fig. 5 shows a

3.3. Microstructural characteristics

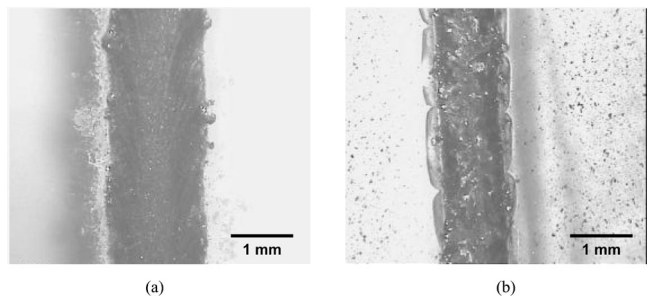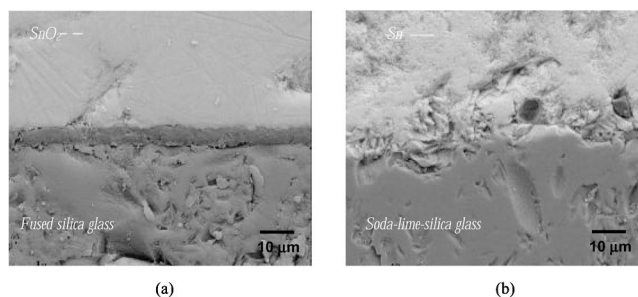The typical cross-sectional microstructure around the interface between SnO$_2$ and (a) fused silica and (b)

Fig. 3. Typical optical surface morphology of SnO$_2$ deposited on (a) fused silica and (b) soda-lime−silica glass.
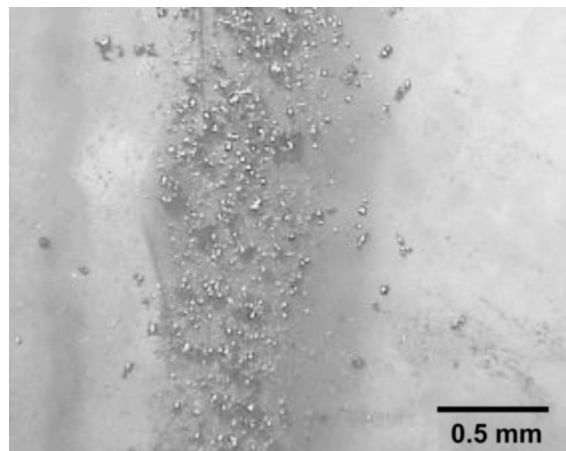

Fig. 5. Typical optical surface view of the phenomena of 'balling' during the deposition of Sn on soda-lime−silica glass.

typical surface view of the balling of Sn on soda-lime–silica glass.

5. Discussion

5.1. Morphological characteristics

As one can see from Fig. 3b, cracking of both the SnO_2 deposited layer and the soda-lime–silica substrate were a common feature of the process. The formation of cracks can be attributed mainly to thermal stresses generated during HPDL irradiation. This is due to the fact that the thermal conductivity SnO_2 is such that, during laser heating, a large thermal gradient between the melt zone and the substrate exists which results in thermal stresses. Additionally, despite the fact that the process of HPDL firing the SnO_2 results from a high specific rate of energy which in turn facilitates localised melting of the SnO_2, the fact that a certain amount of the heat will be conducted to sections of the deposited layer where the SnO_2 is already solidified, combined with the existence of a relatively cold soda-lime–silica glass substrate, means that thermal stresses will be generated. During the heating phase the stresses will be compressive and relieved by plastic deformation, thus precluding crack formation. At high temperatures ($T \geq T_m$) the stresses can also be relieved [20]. On the other hand, during cooling when the temperature falls below T_m, then stresses will accumulate. If the fracture strength of the glass is exceeded then cracking within the melted layer will occur. The thermal stress, σ, induced by a thermal gradient can be calculated using the Kingery equation:

$$\sigma = \frac{E\alpha\Delta T}{1 - \nu} \tag{1}$$

where E is Young's modulus, ΔT is the temperature change, α is the coefficient of thermal expansion and ν is Poisson's ratio. More succinctly, ΔT is the difference between the critical temperature (below which stresses can no longer be relieved) and ambient temperature. For soda-lime–silica glass this is the difference between the melting point of the metals, around 1100°C [20] and ambient temperature 20°C. So, by using the following values for a typical soda-lime–silica glass: $E = 6.42 \times 10^4$ MN m^{-2}, $\alpha = 33 \times 10^{-7}$ K^{-1}, $\Delta T = 1080$°C and $\nu = 0.176$, when the Sn and the SnO_2 were irradiated by the HPDL beam the resulting thermal stress produced in the glass according to Eq. (1) was around 277 MN m^{-2}. Since this is well in excess of the fracture strength of the glass, 120 MN m^{-2} [20], cracking will occur, and can only be avoided by severe distortion or through the reduction of ΔT by pre-heating.
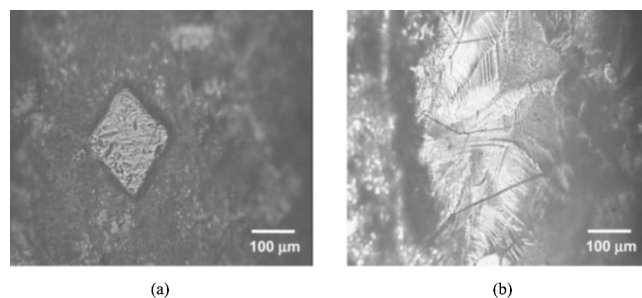

(a)   (b)

Fig. 6. Typical optical surface images of the solidified microstructure of SnO_2 deposited on (a) fused silica and (b) soda-lime–silica glass.

5.2. Solidification microstructures

As can be seen from Fig. 6a, the microstructure obtained on the edges of the deposited tracks appears to be of a fine, elongated cellular nature. In contrast, the microstructures typically observed in the centre of the deposited tracks, as shown in Fig. 6b appear to be semi-ordered dendritic structures.

It is evident from Fig. 6 that the solidification microstructures obtained differed across the same track. Such differences in microstructure within the same track result from the fact that at the edge of the melt track the solidification rate, R, is low while the thermal gradient, G, is at its steepest, therefore G/R is high along the fusion line of the melt pool. Towards the centre of the melt zone the solidification rate is increased while the thermal gradient is reduced. Consequently G/R rapidly falls off as solidification proceeds towards the centre of the melt zone. Thus the high G/R ratio at the interface is just slightly less than that required for stability, that is the degree of constitutional supercooling is smaller, thus different microstructures at the edges of the solidification melt tracks can be formed [21–23].

It is also worthy to note that the formation of the fine elongated structures at the edges of the solidification tracks seen in Fig. 6a could be due to the fact that, although the HPDL beam is not truly Gaussian in nature, the power intensity profile of the beam produces a temperature gradient perpendicular to the direction of traverse [24]. As such, the cooling rate, T, of the SnO_2 will be much faster on the edge of the laser track than in the centre, and may therefore give rise to the much finer and elongated microstructures observed on the edges of the deposited tracks.

The directionally-solidified nature of the microstructure observed on Fig. 3a, which were seen to extend in a perpendicular direction from the edges of the laser melt track, tending inwards towards the centre of the track, is thought to be due to the fact that the HPDL beam intensity is at a maximum in the centre of the profile [25]. For this reason, and because the HPDL beam is circular in shape which results accordingly in

the longest interaction occurring in the centre, the highest temperatures occur in the centre of the track with the lowest temperatures being experienced on the edge of the laser track. Consequently solidification begins at the edges of the track and develops quickly inwards as the laser beam is traversed away. Such observations of directional-solidification are in accord with those of Easterling [26] during welding processes and Bradley et al. [27] during CO_2 laser and HPDL treatment of Al_2O_3 based refractory materials.

5.3. The effects of wettability characteristics

As Fig. 5 shows, it was not possible under any circumstances to deposit pure Sn on any of the glass substrates. It is asserted that this occurrence can be ascribed entirely to the wettability characteristics of the materials. This supposition is borne out somewhat by Fig. 7 which shows an optical micrograph of a sessile drop of (a) SnO_2 and (b) Sn, both at 20°C placed on the surface of fused silica glass with the contact angle superimposed. As one can see from Fig. 7, a considerable difference in the contact angle between both SnO_2 and the Sn and the fused silica glass is observed. Moreover, as is evident from Fig. 7a, the contact angle formed between the Sn and the fused silica glass is in excess of 90°, therefore precluding the possibility of wetting and adhesion occurring [18,19,25].

The particular nature of the wetting characteristics of metal oxides with silicate surfaces is very well documented [10]. The adhesion between glasses and oxides is strong primarily because the two materials are ionic in structure [10]. Nonetheless, the O_2 content of a material's surface is most certainly an influential factor effecting the wetting performance of the material [28,29]. It is perhaps not surprising then that wetting of either glass could not be achieved with the pure Sn since its O_2 content is naturally considerably less than that of SnO_2. Moreover, it is reasonable to conclude that, whereas the O_2 content of the pure Sn is so low that it precludes the material from wetting the selected glasses, the O_2 content of the SnO_2 is sufficiently high for the material to wet and bond to the glasses. Addi-
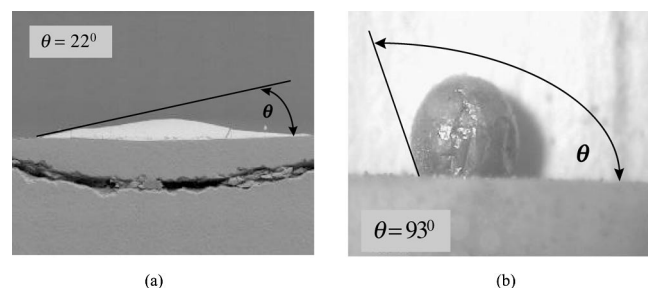

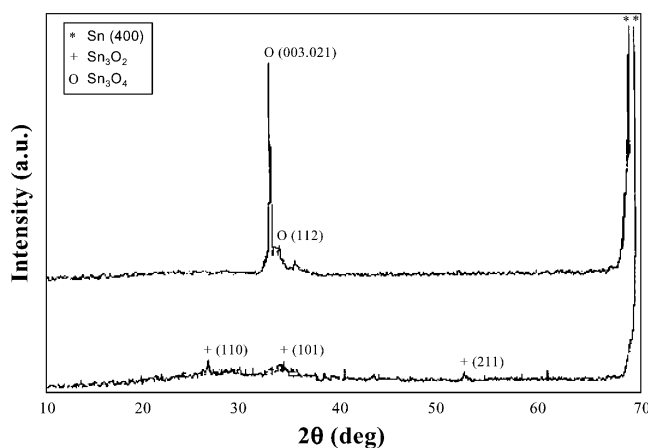Fig. 7. Contact angles for (a) SnO_2 and (b) Sn on the surface of fused silica glass.

Fig. 8. XRD analysis of the deposited SnO_2 layer on fused silica glass (lower plot) and the interface region between the SnO_2 and fused silica glass (upper plot).

tionally, it is important to consider the relative integrities of the glasses during HPDL deposition. As Fig. 3b revealed, the integrity of the soda-lime−silica glass surface could not be kept entirely because of the generated thermal gradients being beyond the glasses strength limits. Consequently cracking occurred which undermined the glass. This constraint for the use of soda-lime−silica glass has being noticed before by Vispute et al. [30].

5.4. Bonding characteristics

From Fig. 4 it is clear that the bonding mechanisms between the SnO_2 and the two glasses are very different. From Fig. 3b the SnO_2 layer exhibits a microstructure characteristic of a mechanical bond. As is evident from Fig. 4b, the mechanical bond generated between the SnO_2 and the soda-lime−silica glass is, as one would expect insofar, as the microstructures of the two materials appear to be interlocking. In this instance it would seem that during the bonding process, the liquid SnO_2 flowed with varying degrees of ease into small cavities and asperities present on the surface of the soda-lime−silica glass. Indeed, such bonds are typical for most oxides on soda-lime−silica glass substrates [10,30]. In Fig. 4a, however, the presence of an interface region between the SnO_2 and the silica glass substrate is clearly visible, indicating the presence of some form of chemical bond. The results of an XRD analysis of the interface region and the deposited SnO_2 layer are shown in Fig. 8. The lower plot shows the results obtained from an analysis within the SnO_2 layer deposited on fused silica glass, whilst the upper plot shows the results of an analysis of the interface region generated between the deposited SnO_2 layer and the fused silica glass. As one can see from the lower plot, the deposited SnO_2 layer, as is to be expected, contains

large amounts of Sn and much smaller amounts of Sn_3O_2. From the lower plot, on the other hand, it can be seen that the generated interface layer is again comprised mainly of Sn, but is also rich in Sn_3O_4. It was therefore possible to deduce that the only difference in the interface layer from the deposited SnO_2 layer was that of Sn_3O_4. It is surmised that this Sn_3O_4 is oxygen enriched SnO_2 resulting from oxide transformation or oxide bridging between the SnO_2 layer and the fused silica glass.

6. Conclusions

The deposition of SnO_2 using a 120-W high power diode laser (HPDL) on both fused silica and soda-lime−silica glass has been successfully demonstrated. Deposition on both glass substrates was carried out with laser power densities of 650−1600 W cm^{-2} and at rates of 420−1550 mm min^{-1}. The maximum theoretical coverage rate that it may be possible to achieve using the HPDL was calculated as being 3.72 m^2 h^{-1}. In contrast, it proved impossible to deposit pure Sn on either glass substrate, with HPDL interaction resulting in the 'balling' of the Sn on the surfaces of the glass. It is asserted that this occurrence is due entirely to differences in the wetting characteristics of the materials, in particular, the differences in the O_2 content of the Sn and the SnO_2. It is believed that the O_2 content of the pure Sn is so low that it precludes the material from wetting the selected glasses, whilst the O_2 content of the SnO_2 is sufficiently high for the material to wet and bond to the glasses.

Evidence of solidified microstructures was observed, with the microstructures differing considerably across the same deposited track. In the centre of the track the microstructure displayed a semi-ordered dendritic structure, whilst on the edge of the track an elongated cell structure was seen. The observed differences in microstructure within the same track can be attributed to the fact that at the edge of the melt pool the solidification rate, R, is low while the thermal gradient, G, is at its steepest, therefore G/R is high along the edge of the laser melt track. Towards the centre of the melt zone the solidification rate is increased while the thermal gradient is reduced. Consequently G/R rapidly falls off as solidification proceeds towards the centre of the melt zone.

The bonding mechanisms between the SnO_2 and the two glasses were found to be very different. Adhesion of the SnO_2 with the soda-lime−silica glass was found

to be due to mechanical bonding. The adhesion of the SnO_2 with the fused silica, on the other hand, was seen to be the result of a chemical bond arising from an interface region between the SnO_2 and the fused silica glass substrate. An XRD analysis of the interface region revealed it to be comprised of mainly Si and rich with Sn_3O_4.

References

[1] V.N. Koinkar, S.B. Ogale, Thin Solid Films 206 (1991) 259.
[2] J.H. Partridge, Glass to Metal Seals, The Society of Glass Technology, Sheffield, 1949.
[3] L. Kazmerski, D. Racine, Thin Solid Films 30 (1975) 19−21.
[4] J. Wallinga, J.D. Ouwen, R.E.I. Schropp, W.F. Vanderweg, Mater. Sci. Forum 173-174 (1995) 1−5.
[5] B. Cohn, Private communication, Nov. 1999.
[6] P. Papadopoulos, Sensors Actuators B34 (1996) 524−527.
[7] D.R. Biswas, Proceedings of SPIE, San Diego, Ca., USA, Vol. 1649,1992, pp 66−74.
[8] R.L. Boxman, S. Goldsmith, Private communication, Oct. 1999.
[9] N. Mori, J. Appl. Phys. 73 (3) (1985) 154−159.
[10] H.K. Pulker, Coatings on Glass, Elsevier, Amsterdam, 1999.
[11] P. Dunbar, I. Birnie, Metal Deposition Techniques, New York, Chapman & Hall, 1983.
[12] P.L. Allen, Proceedings of the BNES Conference on Gas-Cooled Reactors, Sep. 1982, Bristol, UK, 1982, pp. 226−233.
[13] H.M. Phillips, Y. Li, Z. Bi, B. Zhang, Appl. Phys. A 63 (1996) 347−351.
[14] W.M. Steen, Laser Material Processing, Springer-Verlag, London, 1997.
[15] K.Y. Lau, N. Bar-Chaim, I. Ury, C. Harder, A. Yariv, IEEE J. Quantum Elec. 20 (1) (1984) 71−79.
[16] F.F. Hanus, A. Jadin, L.D. Laude, Appl. Surf. Sci. 96-98 (1996) 807−812.
[17] J.D. Flinkfeldt, Optics Laser Tech. 12 (3) (1980) 252−261.
[18] D.L. Bourell, H.L. Marcus, J.W. Barlow, J.J. Beaman, Int. J. Powder Metall. 28 (4) (1992) 369−381.
[19] M. Agarwala, D.L. Bourell, J.J. Beaman, H.L. Marcus, J.W. Barlow, Rapid Prototyping J. 1 (1) (1995) 26−36.
[20] J.D. Ayers, Thin Solid Films 73 (1980) 199−200.
[21] M.C. Flemmings, D.R. Poirer, R.V. Barone, H.D. Brody, J. Iron Steel Inst. 208 (1970) 208−214.
[22] H. Jones, Rapid Solidification of Metals and Alloys, Institute of Metallurgists, London, 1983.
[23] R. Mehrabian, Int. Metals Reviews 27 (4) (1982) 185−209.
[24] J. Mazumder, W.M. Steen, J. Appl. Phys. 51 (2) (1980) 941−947.
[25] J. Lawrence, PhD Thesis, UMIST, 1999.
[26] K.E. Easterling, Introduction to the Physical Metallurgy of Welding, Butterworth-Heinemann, Oxford, 1992.
[27] L. Bradley, L. Li, F.H. Stott, Appl. Surf. Sci. 138-139 (1998) 522−528.
[28] M. Ueki, M. Naka, I. Okamoto, J. Mat. Sci. Lett. 5 (1986) 1261−1262.
[29] J.G. Li, Rare Metals 12 (1993) 84−96.
[30] R.D. Vispute, V.P. Godbole, S.M. Chaudari, S.M. Kanetkar, S.B. Ogale, J. Mater. Res. 3 (6) (1988) 1180−1186.